



Model Updating for Damage Identification: Leveraging Response Surface Methodology and Frequency Response Function Curvature

Nur Raihana Sukri^{1,2}, Nurulakmar Abu Husain^{1,*}, Syarifah Zyrina Nordin¹, Aminudin Abu¹

¹ Malaysia-Japan International Institute of Technology, Universiti Teknologi Malaysia, 54100 Kuala Lumpur, Malaysia

² Jabatan Kejuruteraan Mekanikal, Politeknik Banting Selangor, 42700 Banting, Selangor, Malaysia

ARTICLE INFO

Article history:

Received 16 January 2024

Received in revised form 13 March 2024

Accepted 27 March 2024

Available online 30 April 2024

Keywords:

Structural health monitoring;
experimental modal analysis; response
surface methodology; FRF curvature

ABSTRACT

The limitations of the classical finite element (FE) model updating-based damage identification method, described as having convergence problems and a high computing cost, served as a catalyst for this investigation. Unlike traditional FE models, response surface methodology (RSM) employs explicit mathematical functions to describe the input-response relationship, offering a clear and concise representation. However, the current application of RSM is restricted to a few responses and updating parameters, and unresolved issues persist, including symmetrical damage location and false damage detection. In this study, a new RSM approach is introduced, using FRF curvature as the response. The effectiveness of the proposed method is demonstrated through an experimental modal analysis of a free-free aluminium beam, employing four different Design of Experiment (DOE) techniques: a minimum-run resolution V (CCD_{mr}) design and a half-fractional (CCD_{half}) design using Central Composite Design (CCD), Box-Behnken design (BBD), and D-optimal design. The research systematically evaluates and compares the performance of these DOE techniques in identifying damage. Overall, the results highlight the success of the RSM method, particularly CCD_{half}, D-optimal and BBD, in effectively identifying damage.

1. Introduction

Engineering structures, such as aircraft and bridges, play a vital role in facilitating human activities. These structures are designed to last for decades or even centuries. However, throughout their service life, structural systems are inevitably subjected to damage, leading to potential human and economic losses. Various factors contribute to the degradation of structures, including normal wear and tear, external forces such as weather and natural disasters like earthquakes, which can alter their dimensions and material properties. Different types of damage can influence distinct structural properties, resulting in undesirable stress and vibrations that jeopardize the structural integrity [1].

The diagnosis of structural damage can be achieved through local and global methods [2]. Local methods involve non-destructive testing techniques, such as magnetic testing and visual inspection,

* Corresponding author.

E-mail address: nurulakmar@utm.my

while global methods rely on structural vibrations. With the increasing complexity and size of modern structures, the effectiveness of local methods has diminished [3]. The advent of sensors and transducers has spurred the development of global methods, which have overcome the limitations of local approaches [4].

The global method enables the assessment of the entire structure by analyzing vibration parameters, such as frequency response functions and mode shapes. Any changes in these parameters can show alterations in the structural properties. A commonly used global method is the finite element (FE) model updating strategy [5-7]. This technique involves refining an FE model to rectify discrepancies between numerical and experimental data. The FE model updating can be executed using either a direct or iterative method. The direct method, also referred to as the non-iterative method, involves modifying the system matrix [8]. This method offers computational advantages and produces accurate results. However, it has limited applicability due to the lack of physical interpretation of changes in structural characteristics [9]. On the contrary, the iterative method overcomes the limitations of the direct method, but requires the creation of a sensitivity matrix for all update parameters, which leads to lengthy calculations [5].

This research is motivated by the limitations of the classical FE model updating-based damage identification method, which suffers from convergence issues and high computational costs. To address these challenges, we explore the Response Surface Methodology (RSM), which combines mathematical and statistical approaches. RSM offers an excellent solution to inverse problems without the need for a sensitivity matrix [2]. By employing explicit functions, known as the response surface model (RS), RSM provides a clear and concise explanation of the input-response relationship in structural systems, making it a valuable tool for designing efficient damage identification techniques. However, the current application of RSM is limited to a small number of responses and updating parameters, with most researchers focusing on natural frequencies and mode shapes as responses. Additionally, there are unresolved issues, such as symmetrical damage location and false damage detection [10, 11].

To address the lack of application of model updating-based RSM in damage identification, we enhance existing RSM-based damage identification methods by utilizing frequency response function (FRF) curvature as a response parameter. Damage will only cause subtle shifts in the FRFs, which may go undetected until in-depth analysis of the signals. The FRF curvature, however, will magnify these slight differences [12]. Critically, FRF curvature exhibits heightened sensitivity to changes in the FRF. This distinctive feature positions FRF curvature as a robust candidate for precise and early-stage damage identification. By leveraging FRF curvature, this study seeks to provide a comprehensive and effective solution for structural damage identification, contributing to advancements in the field and enhancing the resilience of critical infrastructures.

2. RSM for Structural Damage Identification

The current RSM-based damage identification method relies on natural frequencies and mode shapes as a response, but suffers from false damage detection issues caused by errors in modeling and response measurement. As a result, the algorithm lacks reliability in accurately localizing damage [13]. Although the FRF exhibits lower measurement errors compared to modal data, it has not been extensively utilized as a response parameter in RSM-based damage identification due to its broad frequency range [14]. Given that response measurement errors significantly impact the accuracy of existing RSM-based damage identification techniques, this study aims to establish procedures for utilizing FRF curvature as a response to provide valuable information for damage identification. The approach of FRF curvature, as developed by Sampaio, Maia [15], has demonstrated its superiority in

damage detection compared to other classical global methods. However, there has been limited research conducted on FRF curvature to date [16, 17].

The RSM, a statistical regression approach, establishes a relationship between design variables and the responses of the system. It aims to identify the optimal combination of design variables through an efficient experimental design with a minimal number of samples [18]. Since the FRF curvature is selected as the response and Young's modulus of each element is chosen as the design variable, the quadratic response surface (RS) model is simplified as:

$$H''(\omega)_{i,j} = \beta_0 + \sum_{i=1}^k \beta_i E_i + \sum_{i < m=2}^k \beta_{im} E_i E_m + \sum_{i=1}^k \beta_{ii} E_i^2 + \varepsilon \quad (1)$$

where k represents the element, $H''(\omega)_{i,j}$ denotes FRF curvature measured at location i for a force input at location j , β_0 β_i β_{im} β_{ii} are the regression coefficients, E_i for Young's modulus, $E_i E_m$ is the design variable interaction components, and E_i^2 denotes the quadratic components.

Figure 1 illustrates the step-by-step process of this study. It starts with the identification of design variables and responses. Experimental modal analysis was conducted to obtain modal parameters for both intact and damaged cases. The experimental results of the intact case were compared with the results obtained from the FE analysis. The initial FE model is modelled using initial Young's modulus (E_i). Model updating of the initial FE model was carried out using RSM, resulting in the creation of the primary RS model. The primary RS model incorporated updated Young's modulus values (E'_i). Subsequently, an assessment of the changes in FRF curvature is conducted for the intact structure. To identify damage, model updating is applied to the secondary RS model. The model updating process yielded the Young's modulus values for each element (E_d), which were then used to calculate the stiffness reduction factor (SRF). The SRF, calculated using Eq. (2), compares the Young's modulus value for the damaged case; E_d , with that of the intact case; E'_i . The SRF serves as an indicator of the severity of the damage, with larger values denoting more substantial damage [13].

$$SRF = 1 - \left(\frac{E_d}{E'_i} \right) \quad (2)$$

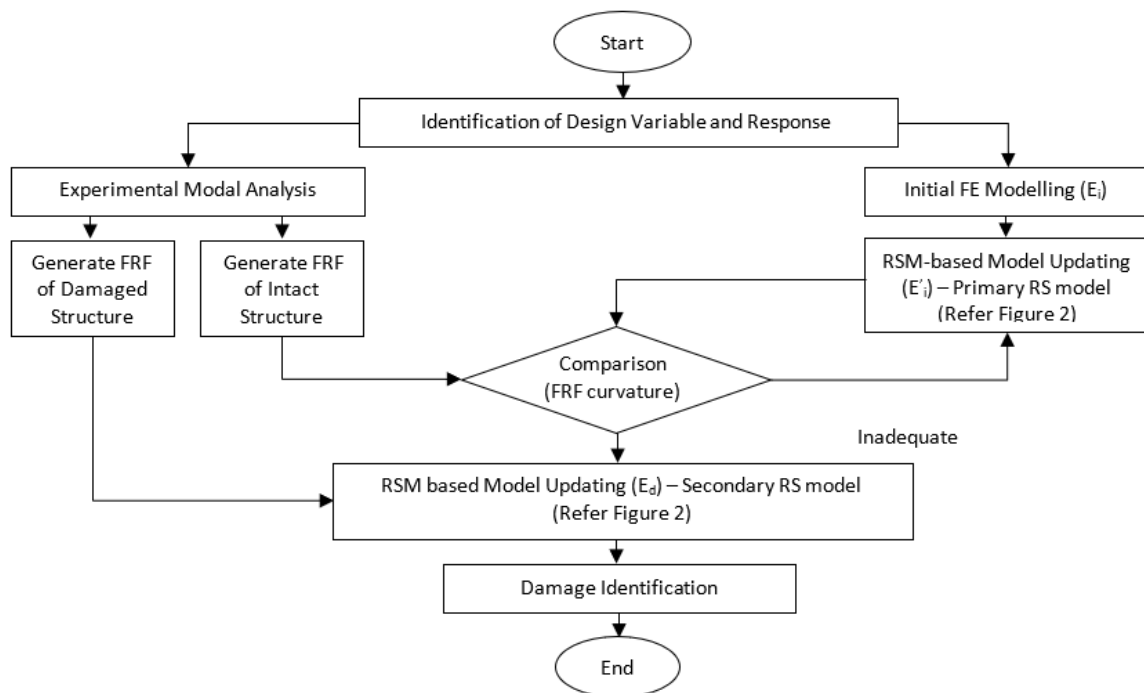


Fig. 1. RSM-based damage identification flow chart using FRF curvature

The details of the process of RSM-based model updating using FRF curvature are illustrated in Figure 2. The Design of Experiment (DOE) process involves selecting the updating design variables and setting the lower and upper bounds for their initial values. Four different DOEs are compared: a minimum-run resolution V (CCDmrv) design and a half-fractional (CCDhalf) design were employed using Central Composite Design (CCD), Box-Behnken design (BBD), and D-Optimal Design (D-Optimal). The FRF curvature response is computed using FE analysis based on the chosen DOE. The FRF curvature is determined at 96% of the first FRF resonance, employing the equation proposed by Sampaio, Maia [15]. Eq. (3) defines the FRF curvature for any given frequency, with $H_{i,j}$ representing the receptance FRF measured at location i for a force input at location j .

$$H''_{i,j} = \frac{H_{i+1,j} - 2H_{i,j} + H_{i-1,j}}{h^2} \quad (3)$$

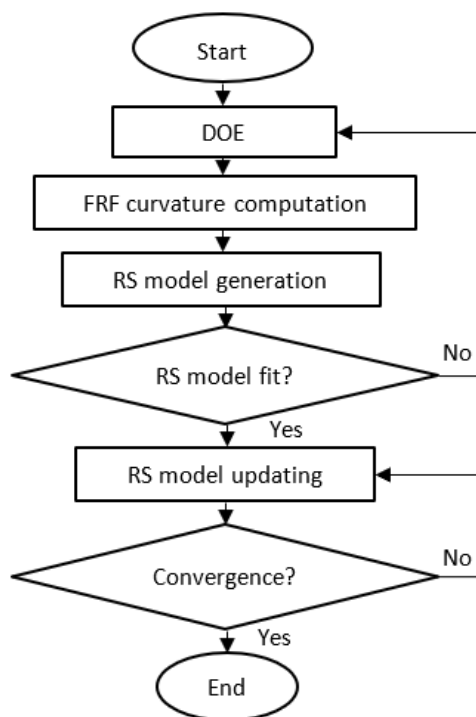


Fig. 2. Flowchart for RSM-based model updating using FRF curvature

Next, the RS model is constructed to establish the relationship between the response and design variables. Quadratic forms are employed in this study to derive the relationship. The generated RS model is then tested against certain criteria, including R-squared (R^2), adjusted R-squared (R^2_{adj}), and predicted R-squared (R^2_{pred}) as defined by Eq. (4), Eq. (5) and Eq. (6), respectively [19, 20]. R^2 represents the amount of dispersion explained by the RS model around the mean [21, 22]. However, the inclusion of insignificant parameter to the model increases the value of R^2 . As a result, the value of R^2_{adj} and R^2_{pred} must be verified. It is important to note that R^2_{pred} measures the model's predictive accuracy, while R^2_{adj} measures the model's ability to explain variation about the mean. Their values should approach 1, with a marginal difference of 0.2 between them. Notably, the values of R^2_{adj} and R^2_{pred} decrease with the inclusion of insignificant parameters [21, 23].

$$R^2 = \left(\frac{SS_R}{SS_T} \right) = 1 - \left(\frac{SS_E}{SS_T} \right), \quad 0 \leq R^2 \leq 1 \quad (4)$$

$$R_{adj}^2 = 1 - \frac{SS_E/(n-p)}{SS_T/(n-1)} = 1 - \frac{n-1}{n-p} (1 - R^2) \quad (5)$$

$$R_{pred}^2 = 1 - \frac{PRESS}{SS_T} \quad (6)$$

After the model is validated, it needs to be updated to match the parameters of the actual structure. The updated design variables are used to determine the location and severity of the damage. A multi-objective optimization problem is formulated as in Eq. (7) to minimize the discrepancy between the FRF curvature obtained from the RS model and the experiment.

$$\min_{x,\gamma} \begin{cases} F(x) - \omega\gamma \leq goal \\ lb \leq x \leq ub \end{cases} \quad (7)$$

where $F(x)$ is the objective function, γ is a dummy variable, and ω is weight to control the attainment of the objectives, $goal$ is the desired value to achieve, lb is the lower bound, and ub is the upper bound. The objective function used in this study is defined in Eq. (8).

$$F(x) = abs\left(\frac{H_{RSM}'' - H_{exp}''}{H_{exp}''}\right) \quad (8)$$

where H_{RSM}'' and H_{exp}'' represent the FRF curvature from the RSM and the experiment, respectively. MATLAB's multi-objective optimization algorithm *fgoalattain* is employed in the updating process. The optimization results provide the values of Young's modulus for each element.

3. Experimental Setup

To reduce the impact of boundary conditions on the test results, a free-free condition was used for both intact and damaged beams. To achieve a nearly ideal free boundary condition, the beams were suspended using soft nylon fishing lines from a steel support frame in the laboratory. The aluminium beam used in the experiment has a length of 1000mm and a cross-section of 0.25m x 0.06m. The beam's material properties include an elastic modulus of 71GPa, a density of 2700kg/m³, and a Poisson's ratio of 0.33. To discretize the beam, it was divided equally into 10 elements and 11 nodes, as illustrated in Figure 3. To evaluate the performance of DOE in identifying damage, saw-cut damages were intentionally introduced at three specific locations, as depicted in Figure 4. The cross section of the damage can be observed in Figure 5.

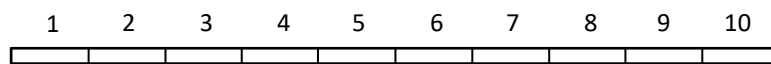


Fig. 3. Free-free aluminum beam

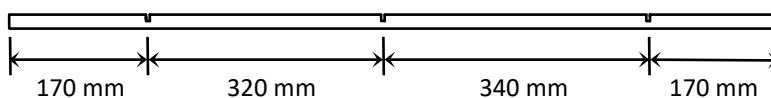


Fig. 4. Damage locations

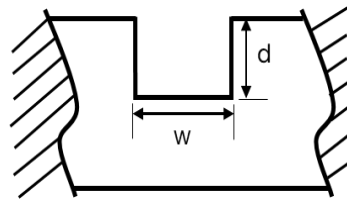


Fig. 5. Damage dimension

Three distinct damage scenarios, namely C1, C2, and C3 as per listed in Table 1, were examined. In the C1 scenario, three saw cuts with a width of 1mm were introduced. In the C2 scenario, three saw cuts with a width of 2mm were implemented. Lastly, the C3 scenario involved three saw cuts with a width of 3mm. The depths of the saw cuts corresponded to 1mm, 2mm, and 3mm of the beam height, respectively.

Table 1

Damage cases		
Scenario	W	D
C1	1 mm	1 mm
C2	2 mm	2 mm
C3	3 mm	3 mm

Figure 6 depicts the experimental setup used in this study, which consists of a Dytran Dytranpulse™ 5800B4 instrumented hammer with sensitivity 10.17 mV/lbf, a Dytran 3133A1 accelerometer with a sensitivity of 10.15493 mV/g and a mass of 0.8 g, a LMS SCADAS Mobile four-channel data acquisition unit and Simcenter Testlab software for signal acquisition and analysis. The responses were measured at 11 nodes along the length of the beam using an accelerometer and the impact hammer was utilized to excite the beam at node 6.

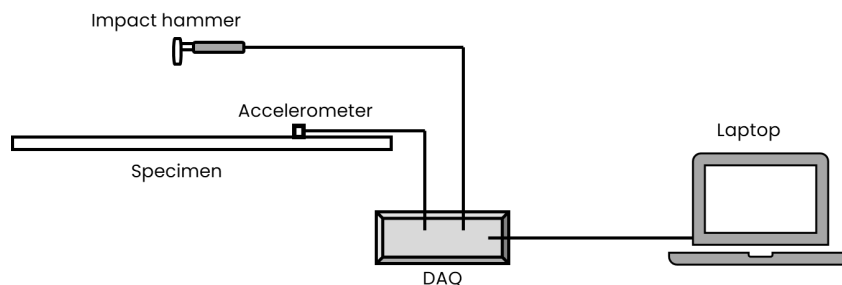


Fig. 6. Schematic diagram of impact hammer modal testing

4. Results

4.1 RSM-based Model Updating of Intact Structure – Primary RS Model

The initial FE model was established using SDTools software to accurately depict the intact configuration of the beam. In this model, the initial Young's modulus value, denoted E_i , was set at 71 GPa. A simulated impact force of 1N was applied at node 6, and SDTools calculated the FRF magnitude for each node. The Design Expert software was utilized to generate the layout for the DOEs. The FRF curvature was then determined at 96% of the first FRF resonance. In the subsequent process to obtain a primary RS model, the E_i values for each element served as the RSM design variables, while the FRF curvatures at nodes 1 to 11 were used as response. The assigned values of $-\alpha$ and $+\alpha$ were 60.35 GPa and 81.65 GPa, respectively, which were equal to $0.85E_i$ and $1.15E_i$. By employing the practical alpha values, -1 and +1 corresponded to 65.0111 GPa and 76.9889 GPa, respectively. CCDhalf consisted of 542 runs with 10 center points, while CCDmrv comprised 82 runs with 6 center

points. In the BBD, the lower and upper boundaries were set at 60.35 GPa and 81.65 GPa, respectively, and the number of center points was 10, resulting in a total of 170 runs. When creating the D-optimal design, the lower and upper boundaries were the same as the BBD, and a coordinate exchange feature was selected to create a full quadratic model D-optimal design. The number of lack of fit was set to 5, and there were no replicates. The calculation for the D-optimal design involved a total of 71 runs.

The RS model utilized in this study was developed based on a full quadratic model. The model criteria for CCDmrv, CCDhalf, BBD, and D-optimal design are presented in Table 2. The R^2 values obtained for all the DOEs indicate a strong fit of the data to the primary RS models, as they are all close to 1. Moreover, the significance of all the parameters considered in this study is confirmed by the values of R^2_{adj} and R^2_{pred} values, which are both close to 1. Additionally, the difference of less than 0.2 between R^2_{adj} and R^2_{pred} further supports the adequacy of the selected parameters. Based on the analysis of the RS model criteria, it can be concluded that the BBD exhibits the most well-fitted RS model, followed by CCDhalf, D-optimal, and CCDmrv in decreasing order of adequacy.

Table 2
 Response surface full quadratic criteria for primary RS model

Response	Criteria	CCDmrv	CCDhalf	BBD	D-Optimal
FRFC node 1	R^2	1.0000	1.0000	1.0000	1.0000
	R^2_{adj}	0.9999	1.0000	1.0000	1.0000
	R^2_{pred}	0.9966	1.0000	1.0000	0.9999
FRFC node 2	R^2	0.9999	0.9996	0.9998	1.0000
	R^2_{adj}	0.9993	0.9995	0.9997	1.0000
	R^2_{pred}	0.9737	0.9994	0.9994	0.9995
FRFC node 3	R^2	1.0000	1.0000	1.0000	1.0000
	R^2_{adj}	0.9999	1.0000	1.0000	1.0000
	R^2_{pred}	0.9968	1.0000	1.0000	0.9995
FRFC node 4	R^2	1.0000	1.0000	1.0000	1.0000
	R^2_{adj}	0.9999	1.0000	1.0000	1.0000
	R^2_{pred}	0.9959	1.0000	1.0000	0.9990
FRFC node 5	R^2	1.0000	1.0000	1.0000	1.0000
	R^2_{adj}	0.9999	1.0000	1.0000	1.0000
	R^2_{pred}	0.9965	1.0000	1.0000	0.9998
FRFC node 6	R^2	1.0000	1.0000	1.0000	1.0000
	R^2_{adj}	0.9999	1.0000	1.0000	1.0000
	R^2_{pred}	0.9948	1.0000	1.0000	0.9999
FRFC node 7	R^2	1.0000	1.0000	1.0000	1.0000
	R^2_{adj}	0.9999	1.0000	1.0000	1.0000
	R^2_{pred}	0.9967	1.0000	1.0000	0.9993
FRFC node 8	R^2	1.0000	1.0000	1.0000	1.0000
	R^2_{adj}	0.9999	1.0000	1.0000	1.0000
	R^2_{pred}	0.9965	1.0000	1.0000	0.9996
FRFC node 9	R^2	1.0000	1.0000	1.0000	1.0000
	R^2_{adj}	0.9999	1.0000	1.0000	1.0000
	R^2_{pred}	0.9966	1.0000	1.0000	0.9992
FRFC node 10	R^2	0.9999	0.9996	0.9997	1.0000
	R^2_{adj}	0.9997	0.9995	0.9996	0.9996
	R^2_{pred}	0.9885	0.9994	0.9992	0.9899
FRFC node 11	R^2	1.0000	1.0000	1.0000	1.0000
	R^2_{adj}	0.9999	1.0000	1.0000	1.0000
	R^2_{pred}	0.9962	1.0000	1.0000	0.9996

The primary RS model constructed from CCDmrv, CCDhalf, BBD, and D-optimal design, was employed to replace the initial FE model. Subsequently, the primary RS model was validated, ensuring that its design variables accurately reflected the responses of the actual structure. To facilitate the optimization process, the updating of design variables was performed using the *fgoalattain* function within MATLAB's multi-objective optimization algorithm. The lower and upper bounds for the design variables were established as 60.35 GPa and 81.65 GPa, respectively. To achieve optimal minimization, a weighting factor, denoted as ω , was assigned a value of 0. The results presented in Figure 7 demonstrate the Young's modulus values, or denoted E'_i , obtained after updating the model through the primary RS models. The E'_i values for each element were then used to generate the secondary RS model specifically for damage identification purposes. Furthermore, Table 3 displays the FRF curvature values obtained when using the E'_i value. The findings reveal that each primary RS model exhibits a satisfactory level of accuracy in predicting the FRF curvature values, albeit with a minor margin of error.

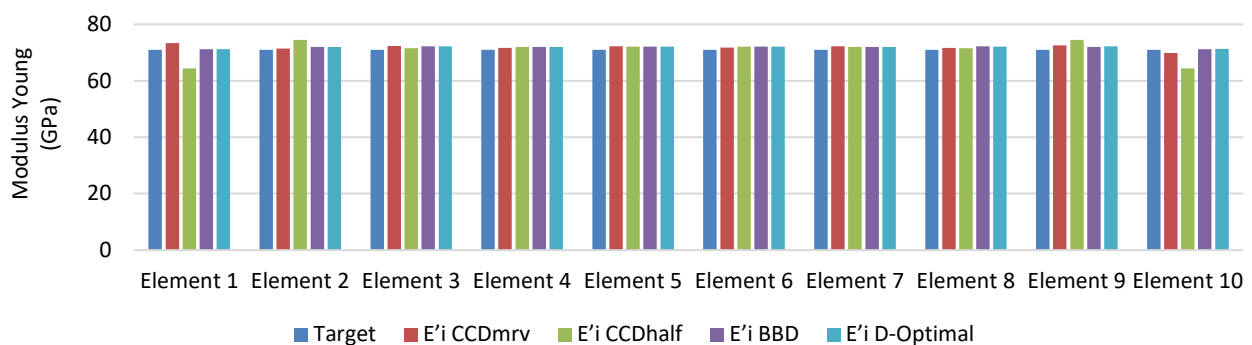


Fig. 7. Young's modulus value after model updating, E'_i

Table 3

FRF curvature value after model updating

Node	Experiment	CCDmrv	Error CCDmrv	CCDhalf	Error CCDhalf	BBD	Error BBD	D-Optimal	Error D-Optimal
N ₁	-2.77E-01	-2.77E-01	0.0%	-2.77E-01	0.0%	-2.77E-01	-0.1%	-2.77E-01	-0.1%
N ₂	4.22E-03	4.22E-03	0.1%	4.23E-03	0.3%	4.22E-03	0.1%	4.22E-03	0.0%
N ₃	9.99E-02	9.99E-02	0.0%	9.98E-02	-0.1%	9.98E-02	-0.1%	9.98E-02	-0.1%
N ₄	2.79E-02	2.79E-02	0.0%	2.79E-02	0.0%	2.78E-02	-0.1%	2.78E-02	0.0%
N ₅	-2.99E-02	-2.99E-02	0.0%	-2.99E-02	0.0%	-2.99E-02	-0.1%	-2.99E-02	-0.1%
N ₆	-3.32E-02	-3.32E-02	0.0%	-3.32E-02	-0.1%	-3.32E-02	-0.1%	-3.32E-02	-0.1%
N ₇	-2.99E-02	-2.99E-02	0.0%	-2.99E-02	0.0%	-2.99E-02	0.0%	-2.99E-02	-0.1%
N ₈	2.79E-02	2.79E-02	0.0%	2.78E-02	0.0%	2.78E-02	-0.1%	2.78E-02	-0.1%
N ₉	9.99E-02	9.99E-02	0.0%	9.98E-02	-0.1%	9.98E-02	-0.1%	9.98E-02	-0.1%
N ₁₀	4.22E-03	4.22E-03	0.1%	4.23E-03	0.3%	4.22E-03	0.0%	4.22E-03	0.0%
N ₁₁	-2.77E-01	-2.77E-01	0.0%	-2.77E-01	0.0%	-2.77E-01	-0.1%	-2.77E-01	-0.1%

4.2 RSM-based Model Updating for Damage Identification – Secondary RS Model

The E'_i values obtained from the primary RS model were utilized to derive a secondary RS model for damage identification. Within the CCD framework, specifically using CCDmrv and CCDhalf designs, the design variables were set as the E'_i values corresponding to each element. The FRF curvatures at nodes 1 to 11 were considered as the response variables. The assigned values of $-\alpha$ and $+\alpha$ were designated as $0.6E'_i$ and E'_i , respectively. CCDhalf comprised 542 runs with 10 center points, while CCDmrv involved 82 runs with 6 center points. Subsequently, the BBD approach was employed for

further analysis. The lower and upper boundaries were defined as $0.6E'_i$ and E'_i , respectively, with 10 center points. Consequently, the BBD design encompassed a total of 170 runs. To create the D-optimal design, the same boundary values as BBD were adopted, and a coordinate exchange feature was utilized to construct a full quadratic model. The lack of fit was set to 5, and no replicates were incorporated into the design. Executing the D-optimal design required 71 runs.

The secondary RS model in this study was based on a comprehensive, full quadratic model. Table 4 presents and analyzes the criteria for CCDmrv, CCDhalf, BBD, and D-optimal designs. The R^2 values obtained for all DOEs indicate a strong agreement between the data and the RS models, approaching 1. This demonstrates a robust fit of the models to the empirical data. Furthermore, the R^2_{adj} and R^2_{pred} values, also close to 1, further affirm the substantial influence of the parameters considered. The small difference between R^2_{adj} and R^2_{pred} , less than 0.2, underscores the careful selection and efficacy of the chosen parameters. According to the analysis, the BBD design stands out as the most well-fitted RS model, whereas the CCDhalf, D-optimal, and CCDmrv designs show slightly less adequacy compared to BBD.

Table 4
 Response surface full quadratic criteria for secondary RS model

Response	Criteria	CCDmrv	CCDhalf	BBD	D-Optimal
FRFC node 1	R^2	0.9999	1.0000	1.0000	1.0000
	R^2_{adj}	0.9992	1.0000	1.0000	0.9999
	R^2_{pred}	0.9712	0.9999	1.0000	0.9975
FRFC node 2	R^2	0.9997	0.9999	0.9999	1.0000
	R^2_{adj}	0.9983	0.9999	0.9999	1.0000
	R^2_{pred}	0.9525	0.9998	0.9998	0.9985
FRFC node 3	R^2	0.9999	1.0000	1.0000	1.0000
	R^2_{adj}	0.9993	1.0000	1.0000	1.0000
	R^2_{pred}	0.9749	0.9999	1.0000	0.9987
FRFC node 4	R^2	0.9998	1.0000	1.0000	1.0000
	R^2_{adj}	0.9991	1.0000	1.0000	0.9999
	R^2_{pred}	0.9667	0.9999	1.0000	0.9981
FRFC node 5	R^2	0.9998	1.0000	1.0000	1.0000
	R^2_{adj}	0.9992	1.0000	1.0000	0.9999
	R^2_{pred}	0.9664	0.9999	1.0000	0.9985
FRFC node 6	R^2	0.9998	1.0000	1.0000	1.0000
	R^2_{adj}	0.9991	1.0000	1.0000	0.9999
	R^2_{pred}	0.9645	0.9999	1.0000	0.9979
FRFC node 7	R^2	0.9998	1.0000	1.0000	1.0000
	R^2_{adj}	0.9990	1.0000	1.0000	0.9999
	R^2_{pred}	0.9682	0.9999	1.0000	0.9976
FRFC node 8	R^2	0.9998	1.0000	1.0000	1.0000
	R^2_{adj}	0.9991	1.0000	1.0000	0.9999
	R^2_{pred}	0.9712	0.9999	1.0000	0.9985
FRFC node 9	R^2	0.9998	1.0000	1.0000	1.0000
	R^2_{adj}	0.9991	1.0000	1.0000	0.9999
	R^2_{pred}	0.9722	0.9999	1.0000	0.9961
FRFC node 10	R^2	0.9998	0.9995	0.9999	1.0000
	R^2_{adj}	0.9990	0.9994	0.9999	0.9995
	R^2_{pred}	0.9651	0.9993	0.9998	0.9854
FRFC node 11	R^2	0.9998	1.0000	1.0000	1.0000
	R^2_{adj}	0.9992	1.0000	1.0000	0.9998
	R^2_{pred}	0.9679	0.9999	1.0000	0.9960

After undergoing validation, the model's design variables were subject to an updating process. The optimization process was similar with the primary model but the lower bound was established as $0.6E'_i$, while the upper bound was defined as E'_i . This process was performed using the measured FRF curvature of the damaged beam. Subsequently, the updated design variables, representing the Young's modulus values for damage state of each element (referred to as E_d), were utilized to accurately ascertain both the location and severity of the structural damage. Figure 8, 9, 10 and 11 show the E_d values obtained by secondary RS models developed from the CCDmrv, CCDhalf, BBD and D-optimal after the model updating process for damage cases C1, C2 and C3.

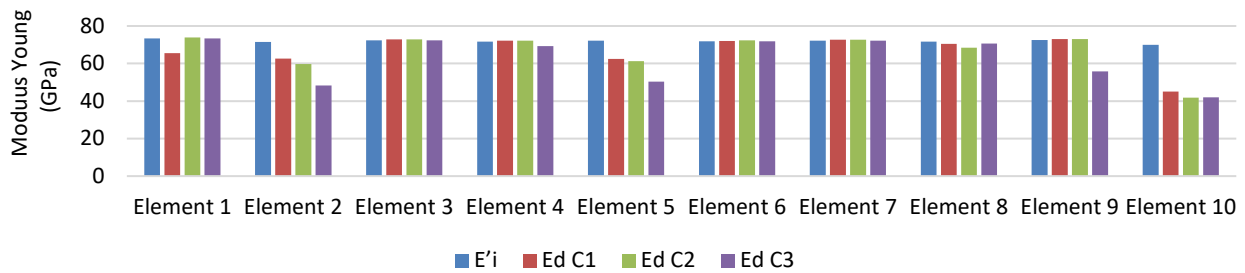


Fig. 8. Young's modulus value, E_d , for CCDmrv

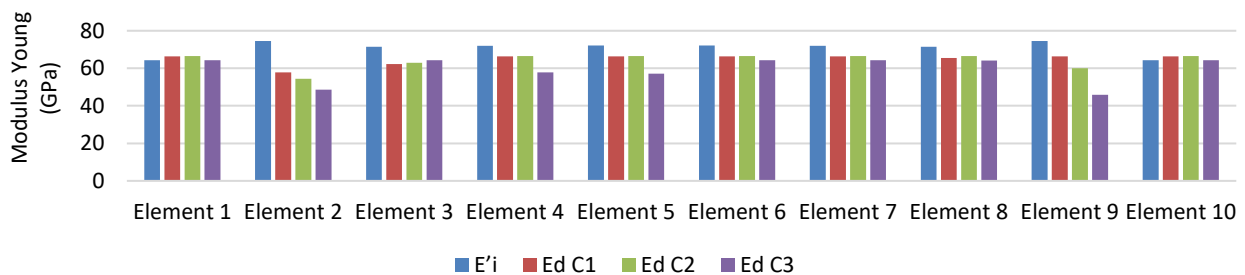


Fig. 9. Young's modulus value, E_d , for CCDhalf

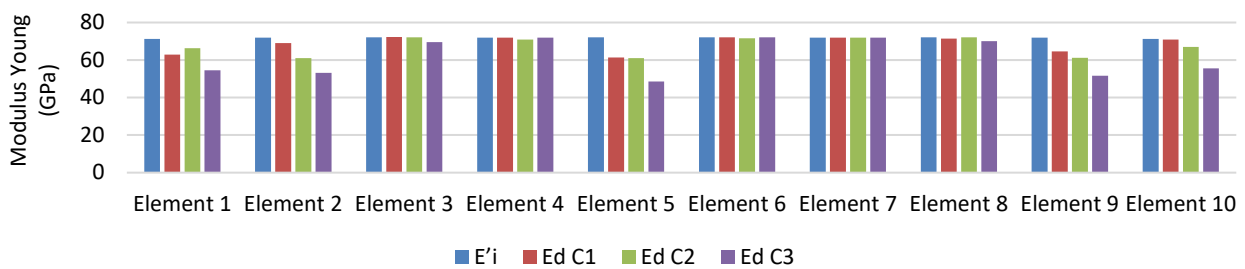


Fig. 10. Young's modulus value, E_d , for BBD

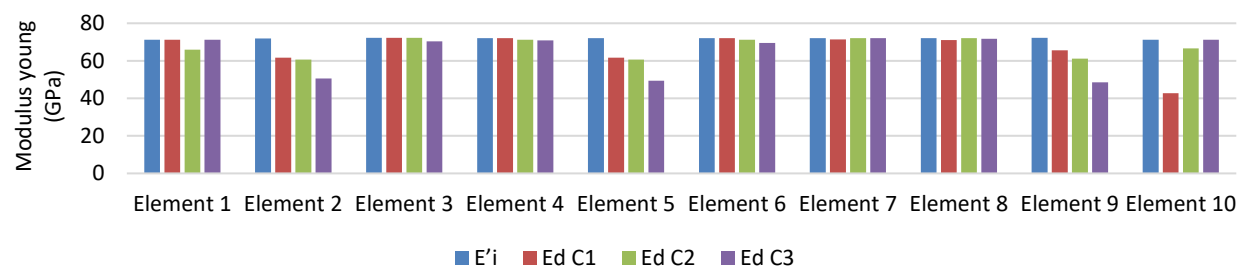


Fig. 11. Young's modulus value, E_d , for D-Optimal

The SRF is an important metric used to assess the severity of structural damage. It quantifies the changes in the stiffness of structural elements and presents the results on a numerical scale, with higher values indicating more significant damage. In this study, the SRF was employed to analyze and quantify the damages in three different cases, namely C1, C2, and C3. The SRF values computed for these cases are visually presented in Figures 12, 13, and 14, respectively. The highlighted elements show the actual damage location. Figure 12 illustrates the outstanding performance of the BBD design in accurately identifying damage for C1, surpassing other designs. In comparison to CCDmrv, CCDhalf, and D-Optimal designs, BBD outperformed in minimizing false damage location, ensuring that the identified damage locations corresponded closely to the true locations within the structure. On the contrary, CCDmrv exhibited limitations in accurately localizing damage, as it encountered challenges in minimizing false damage locations.

Figure 13 demonstrates the remarkable accuracy exhibited by the CCDhalf design in identifying damage for C2, surpassing the performance of CCDmrv, BBD and D-optimal designs. The CCDhalf design demonstrated robustness in the selection of optimal design points, facilitating precise assessment of damage severity and accurate localization of the true damage location. In comparison to CCDmrv, BBD and D-optimal designs, CCDhalf designs significantly minimized the incidence of false damage localization, ensuring close correspondence between the identified damage locations and the actual locations within the structure.

Figure 14 visually demonstrates the exceptional accuracy attained by the D-optimal design methodology in successfully identifying damage for C3, surpassing the performance of BBD, CCDmrv, and CCDhalf designs. By optimizing the selection of design points, the D-optimal design enabled precise assessment of damage severity and accurate localization of the true damage location. Importantly, the D-optimal design showcased a significant reduction in the occurrence of false damage localization when compared to BBD, CCDmrv, and CCDhalf designs. These findings underscore the remarkable accuracy achieved by the D-optimal design, consolidating its position as a reliable and robust approach in improving the reliability of damage identification processes to identify severe damage cases.

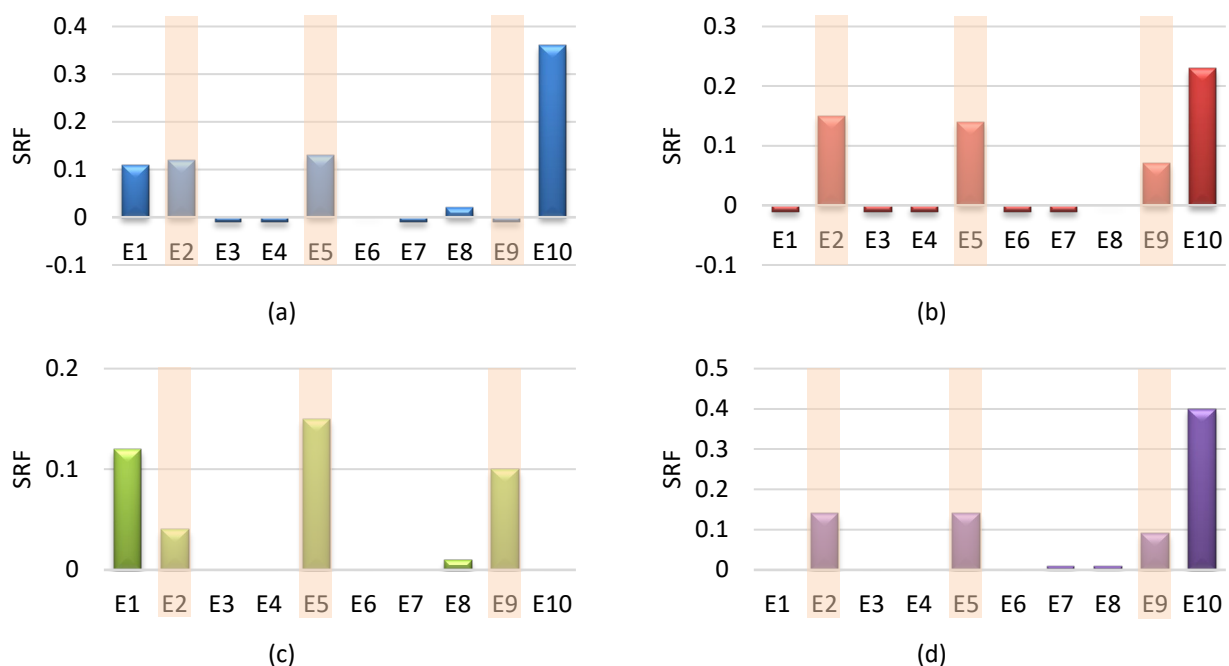


Fig. 12. SRF for damage case C1 (a) CCDmrv (b) CCDhalf (c) BBD (d) D-Optimal

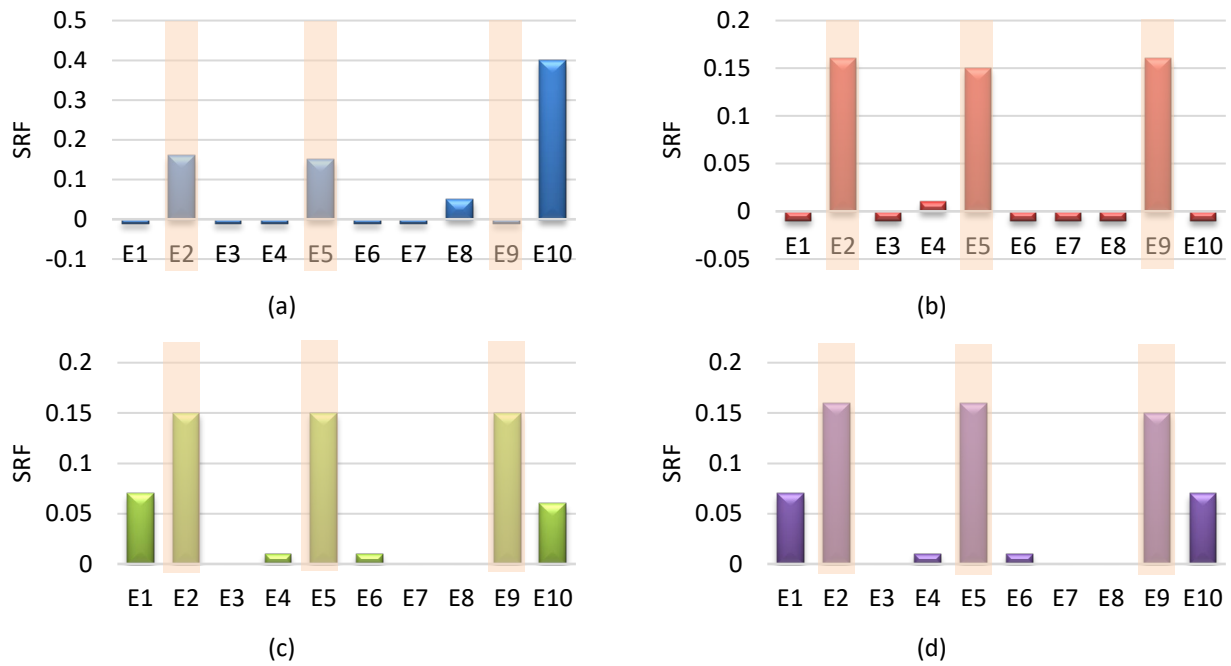


Fig. 13. SRF for damage case C2 (a) CCDmrv (b) CCDhalf (c) BBD (d) D-Optimal

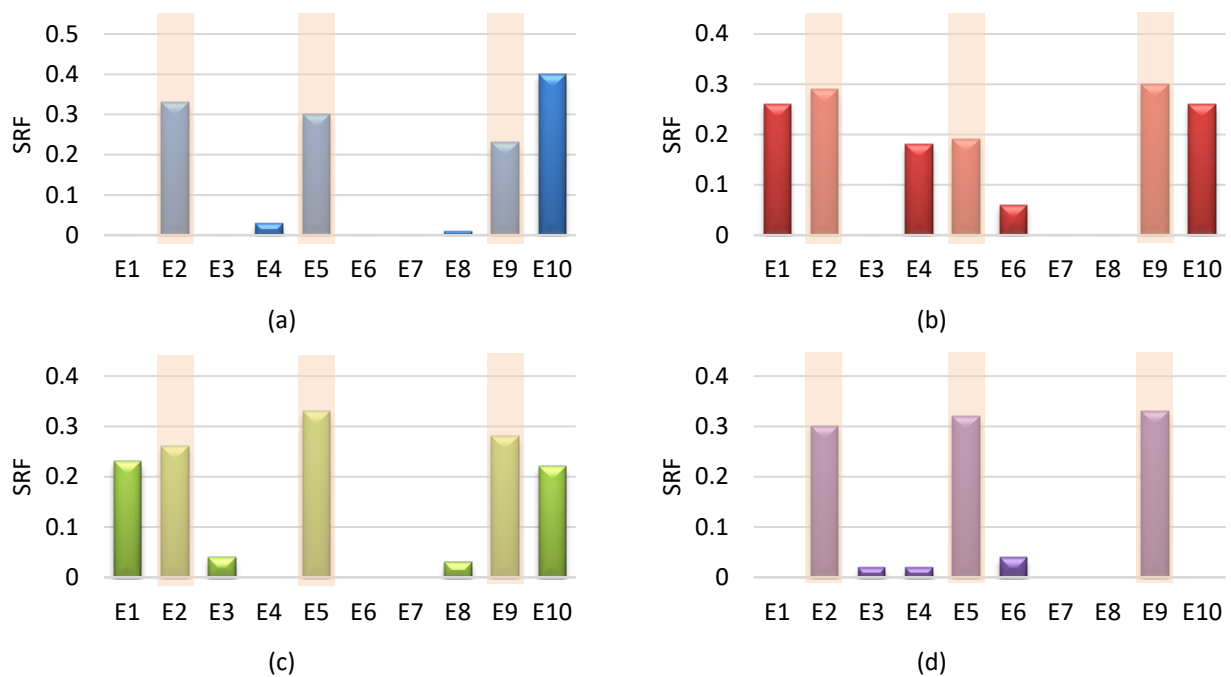


Fig. 14. SRF for damage case C3 (a) CCDmrv (b) CCDhalf (c) BBD (d) D-Optimal

5. Conclusions

In conclusion, this paper presents a novel approach for structural damage identification through the utilization of an RSM-based model updating approach using FRF curvature. Experimental modal analysis conducted on a free-free aluminium beam further validated the efficiency of the RSM approach in identifying damage. The findings of this study demonstrate the effectiveness of the RSM approach, employing various design methodologies, namely CCDmrv, CCDhalf, BBD, and D-optimal design, in identifying damage in three damage severity cases. CCDhalf showcased commendable

ability in identifying multiple damage locations, exhibiting enhanced reliability when dealing with smaller damage scenarios compared to severe damage cases. In contrast, CCDmrv showed limitations in accurately localizing damage, with an error rate of around 40% for all damage cases.

On the other hand, BBD proved effective in identifying small damage cases, albeit with some occurrences of false damage localization, with errors of less than 7%. The D-optimal design, in turn, demonstrated accurate identification of severe damage, while also showing minor instances of false damage localization with an error rate of less than 4%. However, for small damage cases, it did exhibit some challenges in accurately pinpointing the true damage locations. These observations provide valuable information on the strengths and limitations of each design methodology, enabling practitioners and researchers to make informed decisions when selecting the most appropriate approach for the identification of damage based on the specific characteristics and severity of the damage under consideration.

Overall, the results highlight the success of the RSM method, particularly CCDhalf, D-optimal and BBD, in effectively identifying damage while minimizing the occurrence of false damage localization. However, additional experimentation is necessary to thoroughly investigate the influence of measurement points on the effectiveness and overall performance of the proposed method. Such investigations will provide valuable information and enable the refinement of the proposed method, leading to its enhanced applicability and effectiveness in practical applications.

Acknowledgement

The research was funded by the Ministry of Higher Education (MOHE) under the Fundamental Research Grant Scheme (FRGS), UTM, FRGS/1/2022/TK10/UTM/02/41 and supported by Universiti Teknologi Malaysia (UTM). The first author was funded by the Ministry of Higher Education of Malaysia under Hadiah Latihan Persekutuan (HLP).

References

- [1] Gharehbaghi, Vahid Reza, Ehsan Noroozinejad Farsangi, Mohammad Noori, Tony Y. Yang, Shaofan Li, Andy Nguyen, Christian Málaga-Chuquitaype, Paolo Gardoni, and Seyedali Mirjalili. "A critical review on structural health monitoring: Definitions, methods, and perspectives." *Archives of computational methods in engineering* 29, no. 4 (2022): 2209-2235. <https://doi.org/10.1007/s11831-021-09665-9>
- [2] Hou, Rongrong, and Yong Xia. "Review on the new development of vibration-based damage identification for civil engineering structures: 2010–2019." *Journal of Sound and Vibration* 491 (2021): 115741. <https://doi.org/10.1016/j.jsv.2020.115741>
- [3] An, Yonghui, Eleni Chatzi, Sung-Han Sim, Simon Laflamme, Bartłomiej Blachowski, and Jinping Ou. "Recent progress and future trends on damage identification methods for bridge structures." *Structural Control and Health Monitoring* 26, no. 10 (2019): e2416. <https://doi.org/10.1002/stc.2416>
- [4] Alkayem, Nizar Faisal, Maosen Cao, and Minvydas Ragulskis. "Damage diagnosis in 3D structures using a novel hybrid multiobjective optimization and FE model updating framework." *Complexity* 2018 (2018). <https://doi.org/10.1155/2018/3541676>
- [5] Mottershead, John E., Michael Link, and Michael I. Friswell. "The sensitivity method in finite element model updating: A tutorial." *Mechanical systems and signal processing* 25, no. 7 (2011): 2275-2296. <https://doi.org/10.1016/j.ymsp.2010.10.012>
- [6] Sukri, Nur Raihana, Nurulakmar Abu Husain, Syarifah Zyurina Nordin, and Mohd Shahrir Mohd Sani. "Structural Damage Identification Using Model Updating Approach: A Review." *Journal of Advanced Research in Applied Mechanics* 84, no. 1 (2021): 1-12.
- [7] Ereiz, Suzana, Ivan Duvnjak, and Javier Fernando Jiménez-Alonso. "Review of finite element model updating methods for structural applications." In *Structures*, vol. 41, pp. 684-723. Elsevier, 2022. <https://doi.org/10.1016/j.istruc.2022.05.041>
- [8] Bagha, Ashok Kumar, Prashant Gupta, and Varun Panwar. "Finite element model updating of a composite material beam using direct updating method." *Materials Today: Proceedings* 27 (2020): 1947-1950. <https://doi.org/10.1016/j.matpr.2019.09.024>

- [9] Alkayem, Nizar Faisal, Maosen Cao, Yufeng Zhang, Mahmoud Bayat, and Zhongqing Su. "Structural damage detection using finite element model updating with evolutionary algorithms: a survey." *Neural Computing and Applications* 30 (2018): 389-411. <https://doi.org/10.1007/s00521-017-3284-1>
- [10] Alpaslan, Emre, Kemal Haciefendioğlu, Gökhan Demir, and Fahri Birinci. "Response surface-based finite-element model updating of a historic masonry minaret for operational modal analysis." *The Structural Design of Tall and Special Buildings* 29, no. 9 (2020): e1733. <https://doi.org/10.1002/tal.1733>
- [11] Mukhopadhyay, Tanmoy, Tushar Kanti Dey, Rajib Chowdhury, and Anupam Chakrabarti. "Structural damage identification using response surface-based multi-objective optimization: a comparative study." *Arabian Journal for Science and Engineering* 40 (2015): 1027-1044. <https://doi.org/10.1007/s13369-015-1591-3>
- [12] Mondal, Subhajit, Bidyut Mondal, Anila Bhutia, and Sushanta Chakraborty. "Damage detection in beams using frequency response function curvatures near resonating frequencies." In *Advances in Structural Engineering: Dynamics, Volume Two*, pp. 1563-1573. Springer India, 2015. https://doi.org/10.1007/978-81-322-2193-7_119
- [13] Umar, Sarehati, Norhisham Bakhary, and A. R. Z. Abidin. "Response surface methodology for damage detection using frequency and mode shape." *Measurement* 115 (2018): 258-268. <https://doi.org/10.1016/j.measurement.2017.10.047>
- [14] Yang, Xiuming, Xinglin Guo, Huajiang Ouyang, and Dongsheng Li. "A Kriging model based finite element model updating method for damage detection." *Applied Sciences* 7, no. 10 (2017): 1039. <https://doi.org/10.3390/app7101039>
- [15] Sampaio, R. P. C., N. M. M. Maia, and J. M. M. Silva. "Damage detection using the frequency-response-function curvature method." *Journal of sound and vibration* 226, no. 5 (1999): 1029-1042. <https://doi.org/10.1006/jsvi.1999.2340>
- [16] Porcu, M. C., D. M. Patteri, S. Melis, and F. Aymerich. "Effectiveness of the FRF curvature technique for structural health monitoring." *Construction and Building Materials* 226 (2019): 173-187. <https://doi.org/10.1016/j.conbuildmat.2019.07.123>
- [17] Nayyar, Ayisha, Ummul Baneen, Syed Abbas Zilqurnain Naqvi, and Muhammad Ahsan. "Detection and localization of multiple small damages in beam." *Advances in Mechanical Engineering* 13, no. 1 (2021): 1687814020987329. <https://doi.org/10.1177/1687814020987329>
- [18] ADean, Angela, Daniel Voss, Danel Draguljić, Angela Dean, Daniel Voss, and Danel Draguljić. "Response surface methodology." *Design and analysis of experiments* (2017): 565-614. https://doi.org/10.1007/978-3-319-52250-0_16
- [19] Shimpi, Vinay, Madappa VR Sivasubramanian, and S. B. Singh. "Integrating response surface methodology and finite element analysis for model updating and damage assessment of multi-arch gallery masonry bridges." *Sādhanā* 49, no. 1 (2024): 33. <https://doi.org/10.1007/s12046-023-02363-1>
- [20] Patel, Bhawna, and U. K. Dewangan. "Development of Response Surface Model for the Damage Identification of Cantilever Beam." *Civil Engineering and Architecture* 11, no. 5 (2023): 2461-2468. <https://doi.org/10.13189/cea.2023.110516>
- [21] Fang, Sheng-En, and Ricardo Perera. "A response surface methodology based damage identification technique." *Smart Materials and Structures* 18, no. 6 (2009): 065009. <https://doi.org/10.1088/0964-1726/18/6/065009>
- [22] Wah, William Soo Lon, Yung-Tsang Chen, and John S. Owen. "A regression-based damage detection method for structures subjected to changing environmental and operational conditions." *Engineering Structures* 228 (2021): 111462. <https://doi.org/10.1016/j.engstruct.2020.111462>
- [23] Anjneya, Kumar, and Koushik Roy. "Response surface-based structural damage identification using dynamic responses." In *Structures*, vol. 29, pp. 1047-1058. Elsevier, 2021. <https://doi.org/10.1016/j.istruc.2020.11.033>